Supporting information

3D Hierarchical Porous Indium Catalyst for Highly Efficient Electroreduction of CO_2

Wen Luo,[a,b] Wei Xie,[c] Mo Li, [a,b] Jie Zhang, [a,b] Andreas Züttel[a,b]*

a. Laboratory of Materials for Renewable Energy (LMER), Institute of Chemical Sciences and Engineering (ISIC), Basic Science Faculty (SB), École Polytechnique Fédérale de Lausanne (EPFL) Valais/Wallis, Energypolis, Rue de l'Industrie 17, CH-1951 Sion, Switzerland

b. Empa Materials Science & Technology, CH-8600 Dübendorf, Switzerland

c. INAMORI Frontier Research Center, Kyushu University, 744 Motooka, Nishiku, Fukuoka 819-0395, Japan

Corresponding author:wen.luo@epfl.ch

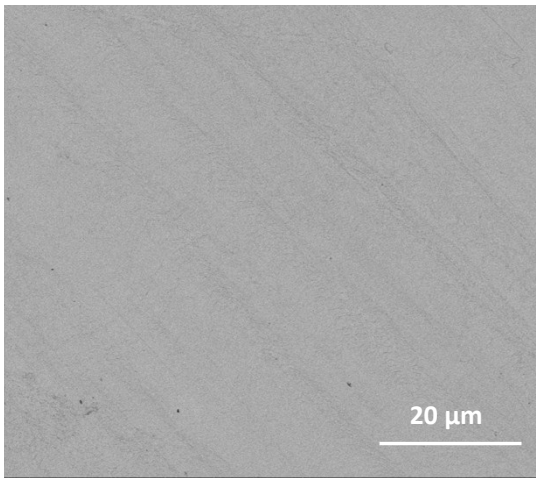

Figure S1 SEM image of the cleaned In foil sample

Table S1 Mass loading of *hp*-In, Pd-In and porous Pd samples measured by ICP-OES.

Sample	*hp*-In	Pd-In-0.1	Pd-In-0.5	Pd-In-1.0	Pd-In-2.0	Porous Pd
Mass of In (mg/cm^2)	13.3	13.1	13.0	13.4	13.5	-
Mass of Pd (mg/cm^2)	-	1.4 E-2	3.1 E-2	5.2 E-2	9.9 E-2	1.7 E-1

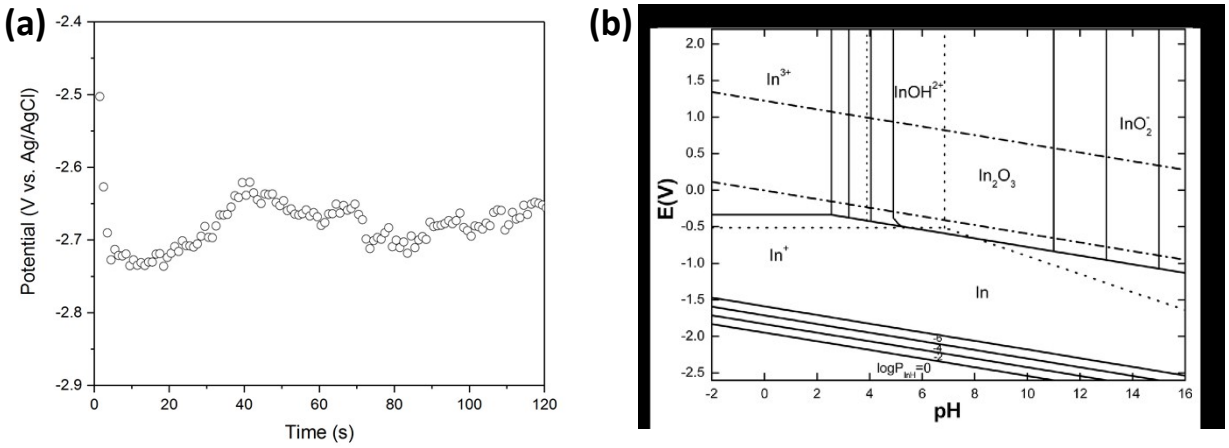

Figure S2 (a) Potential as a function of time for electrodeposition of *hp*-In. (b) Purbaix diagram (E vs. pH diagram) for indium in water at 25 ^{o}C.[1,2] Figure S2 a shows that during the electrodeposition, the applied voltage was extremely low (around -2.7 V vs. Ag/AgCl, which is about -2.5 V vs. SHE). Compared with the Pourbaix diagram shown in Figure S2 b, under our deposition condition, no indium oxide or hydroxide can form.

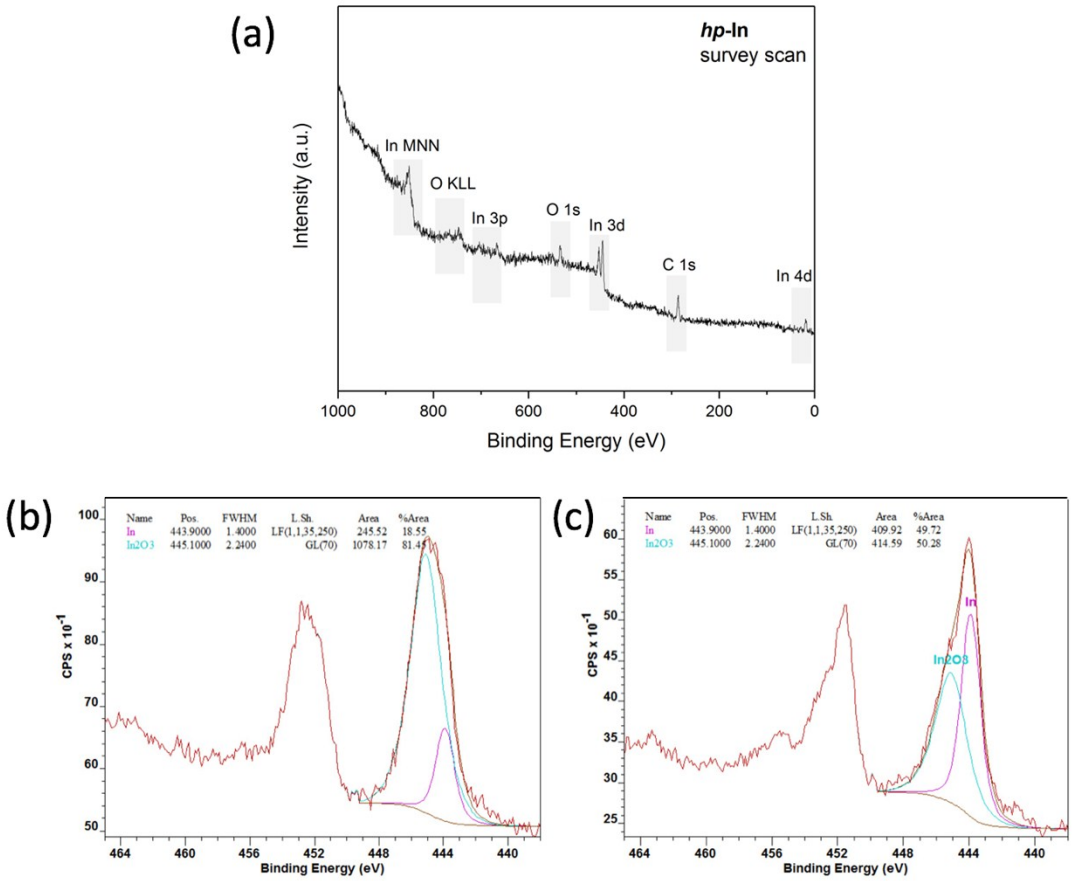

Figure S3 (a) XPS survey scan of as-prepared *hp*-In, and XPS deconvolution parameters of (b) In foil and (c) *hp*-In.

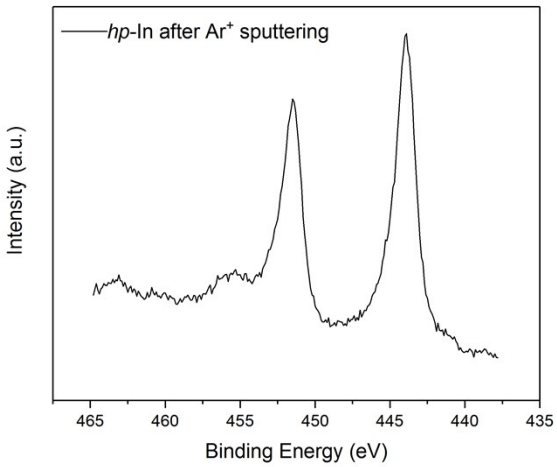

Figure S4 In 3d XP spectrum of *hp*-In after Ar^+ sputtering.

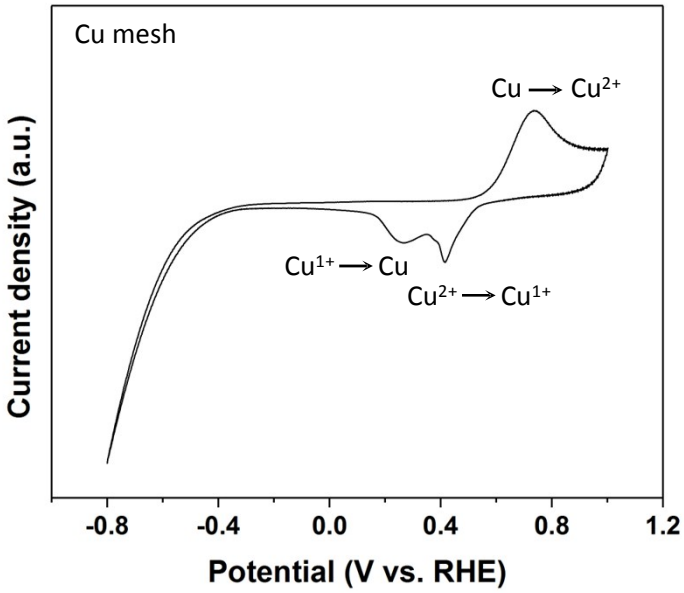

Figure S5 CV of Cu mesh performed in CO_2 saturated 0.1 M $KHCO_3$ (scan rate 50 mV/s). The redox peaks of Cu appear at higher potential range compared with those of In.

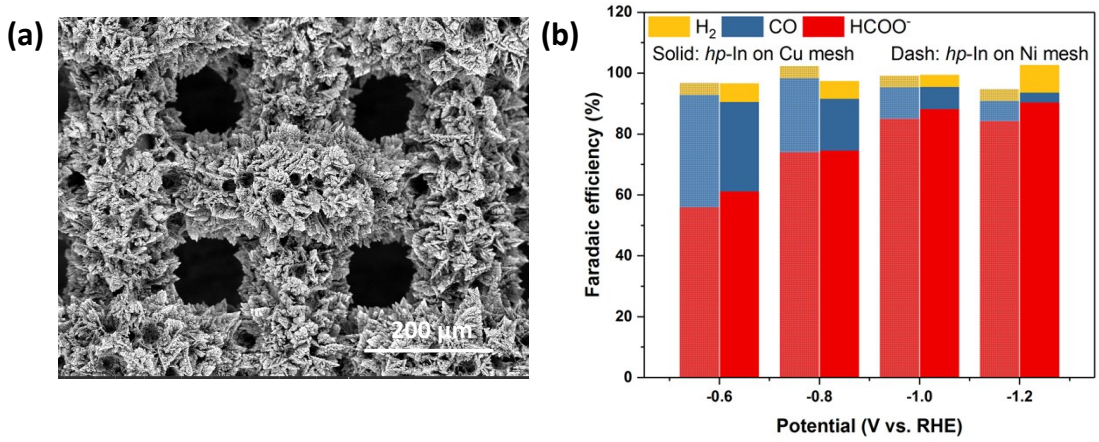

Figure S6 (a) SEM image of porous In deposited on Ni mesh. (b) Potential dependent faradaic efficiencies for *hp*-In on Cu mesh and porous In on Ni mesh.

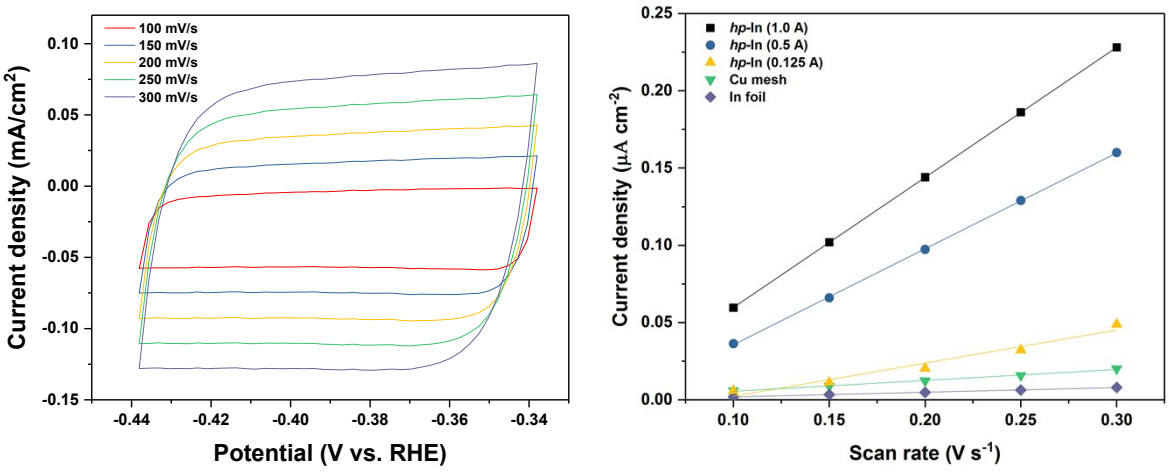

Figure S7 CVs for the *hp*-In at various scan rates (left). The linear regression of the double layer capacitance of each material obtained from the electrochemical studies (right).

Table S2 Summary of the roughness factors of the four In electrodes and the Cu mesh substrate used in this work.

Electrode	Capacitance	Electrochemical surface area (cm^2)
In foil	30.5 μF	1
Cu mesh	71.0 μF	2
hp-In (0.125 A)	0.22 mF	7.1
hp-In (0.5 A)	0.62 mF	20.3
hp-In (1.0 A)	0.84 mF	27.6

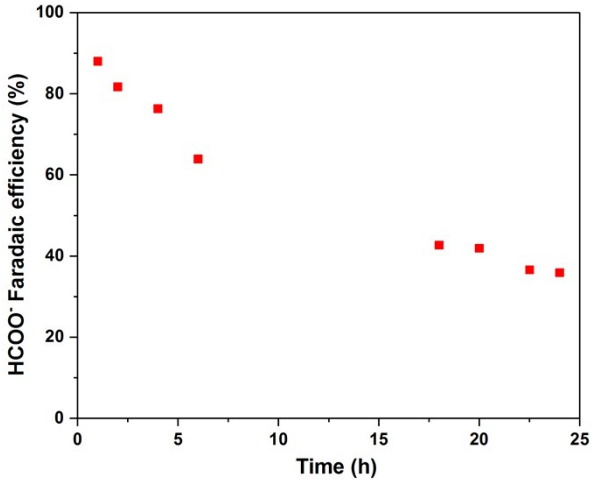

Figure S8 Stability of *hp*-In, tested without exchanging the electrolyte.

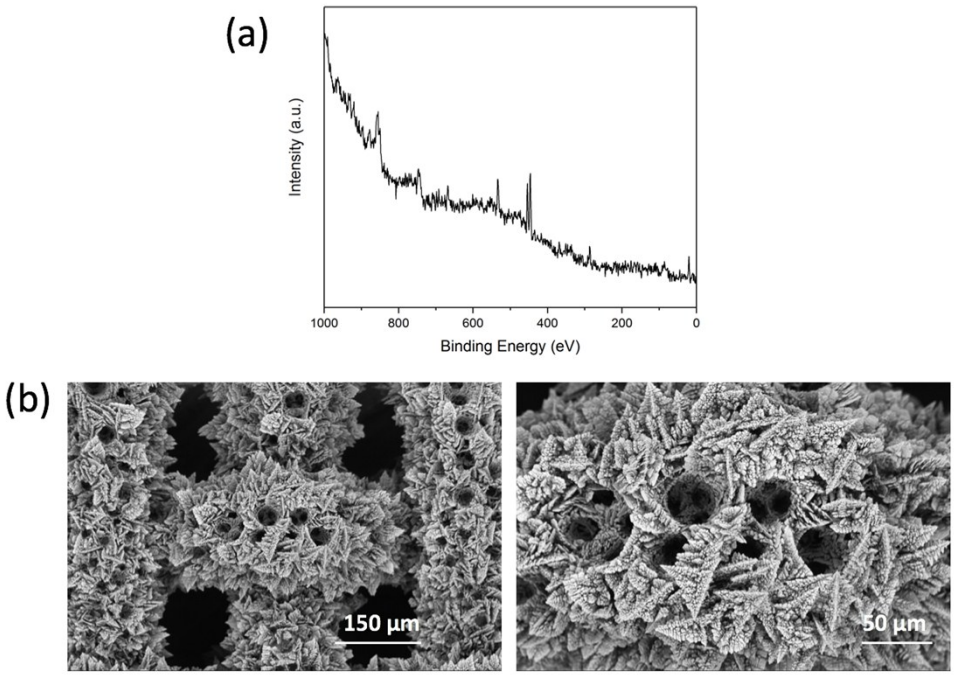

Figure S9 (a) XPS survey scan (b) SEM images of *hp*-In after 24 h stability test. No Cu from Cu mesh can be detected by XPS. SEM images show similar 3D structure as that of the fresh *hp*-In sample.

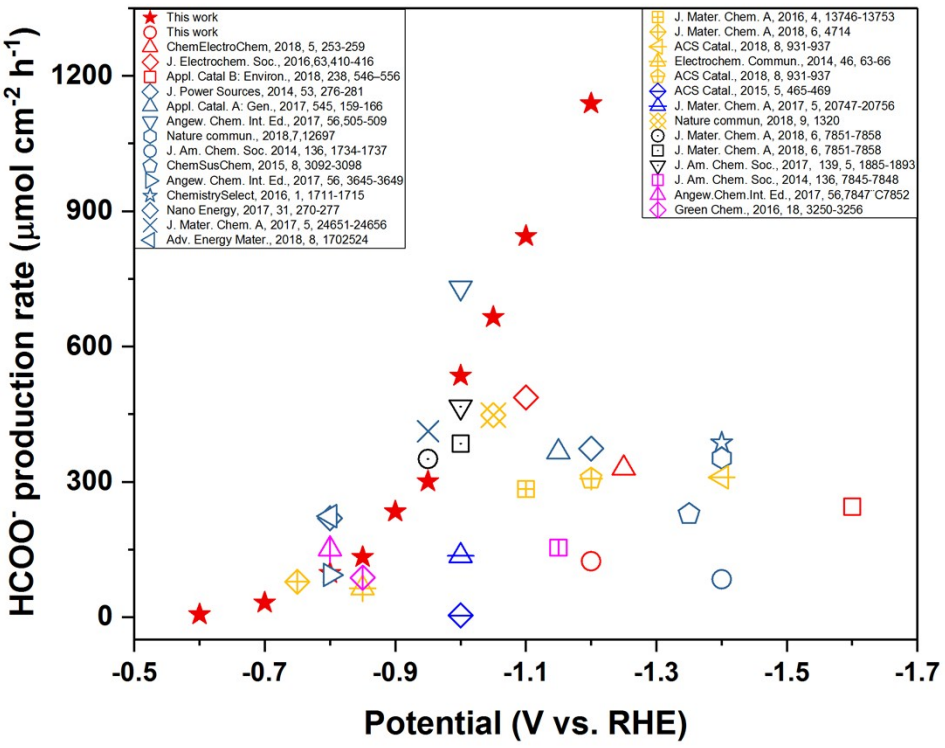

Figure S10 Formate production rate at various applied potentials on the *hp*-In electrode, along with an overview of the formate production rate on the state-of-the-art CO_2-to-formate catalysts.

Table S3 Comparison of CO_2 reduction performance on different In-based catalysts.

Electrode	Electrolyte	Operating potential (vs. RHE)	Current density (mA/cm^2)	Faradaic efficiency for formate	Reference
***hp*-In**	**0.1 M $KHCO_3$**	**-1.0 V -1.2 V**	**32.5 67.5**	**89.1% 90.4%**	**This work**
In/C GDE	0.1 M Na_2SO_4	-1.05 V	6.3	45%	[3]
In/Graphite	0.05 M $NaHCO_3$	-1.6 V	~ 18.5[a]	94.5%	[4]
Dendritic In	0.5 M $KHCO_3$	-0.86 V	5.8	86%	[5]
Anodized In	0.5 M Na_2SO_4	-1.2 V	-	~ 88%[a]	[6]
$In(OH)_3$/C	0.5 M K_2SO_4	-1.1 V	~5.4[a]	70% -77%	[7]
In nanoparticle	0.5 M K_2SO_4	-0.85 V	~2[a]	~100%	[8]
In nanocrystal	Ion liquid (AN-BMIMPF6 solution)	-1.9 V (SCE)	~15	~99% (CO)	[9]

[a] This value is derived from the graphical results in the article.

Table S4 Optimized adsorption configurations of *H, *COOH and *OCHO on three facets of In.

	002	110	112
*H	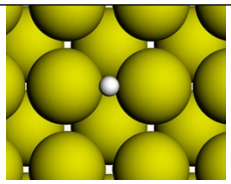	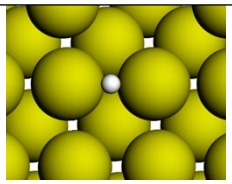	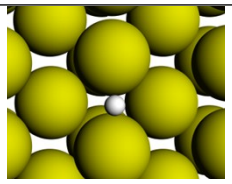
*COOH	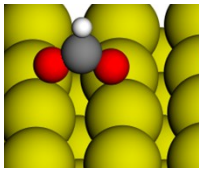	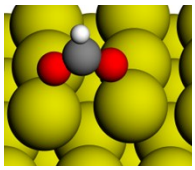	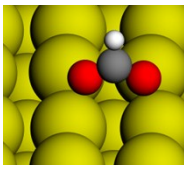
*OCHO	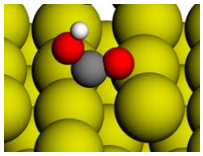	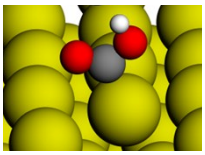	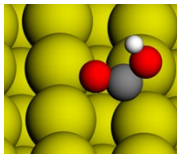

Table S5 The zero-point energy correction (E_{ZPE}), enthalpy correction ($\int C_v\,dT$), and entropy correction (-TS) for adsorbates on three different structures. All values are given in eV.

Structure	Adsorbates	E_{ZPE}	$\int C_v\,dT$	-TS
In(101)	*COOH	0.60	0.24	-0.89
	*OCHO	0.59	0.23	-0.94
In(002)	*COOH	0.59	0.24	-0.88
	*OCHO	0.60	0.23	-0.88
In(110)	*COOH	0.59	0.24	-0.89
	*OCHO	0.59	0.21	-0.83
In(112)	*COOH	0.59	0.24	-0.89
	*OCHO	0.60	0.23	-0.89

Table S6 The zero-point energy correction (E_{ZPE}), enthalpy correction ($\int Cv\, dT$), and entropy correction (-TS) for free gaseous molecules with their partial pressure of 101325 Pa except for H_2O and HCOOH. In the case of H_2O, 3534 Pa was used and 2 Pa was used for HCOOH. Gas phase corrections were applied to CO_2, CO and HCOOH with the value of 0.13, -0.54 and -0.1 eV, repectively.[10] All values are given in eV.

Species	E_{ZPE}	$\int Cv\, dT$	-TS	G- E_{DFT}
CO_2	0.31	0.14	-0.64	-0.19
CO	0.14	0.12	-0.60	-0.34
H_2O	0.58	0.11	-0.53	0.17
H_2	0.28	0.11	-0.45	-0.06
HCOOH	0.90	0.18	-0.69	0.39

Table S7 Calculated DFT energies for HER.[a]

Species	E_{DFT}
H_2 (g)	-6.81
In(101)	-65.92
H*	-68.64
In(002)	-29.13
H*	-31.89
In(110)	-28.78
H*	-31.54
In(112)	-27.67
H*	-30.51

[a] The HER free energy G_{H*} is determined as $G_{H*} = E[surf + H] - E[surf] - E[H_2]/2 + \Delta E_{ZPE} - TS$. Where E[surf + H] and E[surf] are the total energies of the surface with and without the H adsorbate, respectively. $E[H_2]$ is the total energy of a hydrogen molecule. ΔE_{ZPE} is the difference in the zero-point energy between the adsorbed H atom and the gaseous phase H_2. S is the difference in entropy. At T = 298 K, G_{H*} can be calculated by $G_{H*} = E[surf + H] - E[surf] - E[H_2]/2 + 0.24$ eV. [10,11]

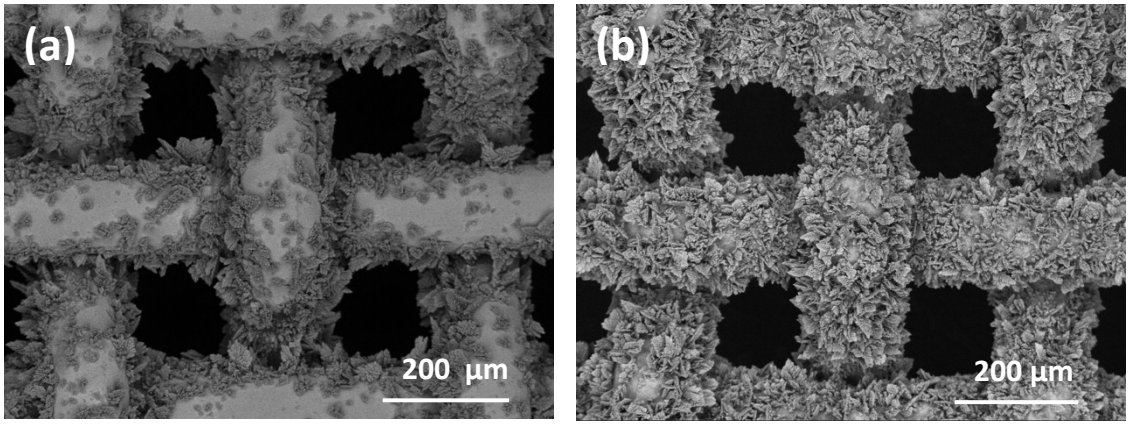

Figure S11 SEM images of as-prepared (a) *hp*-In-0.125 and (b) *hp*-In-0.5.

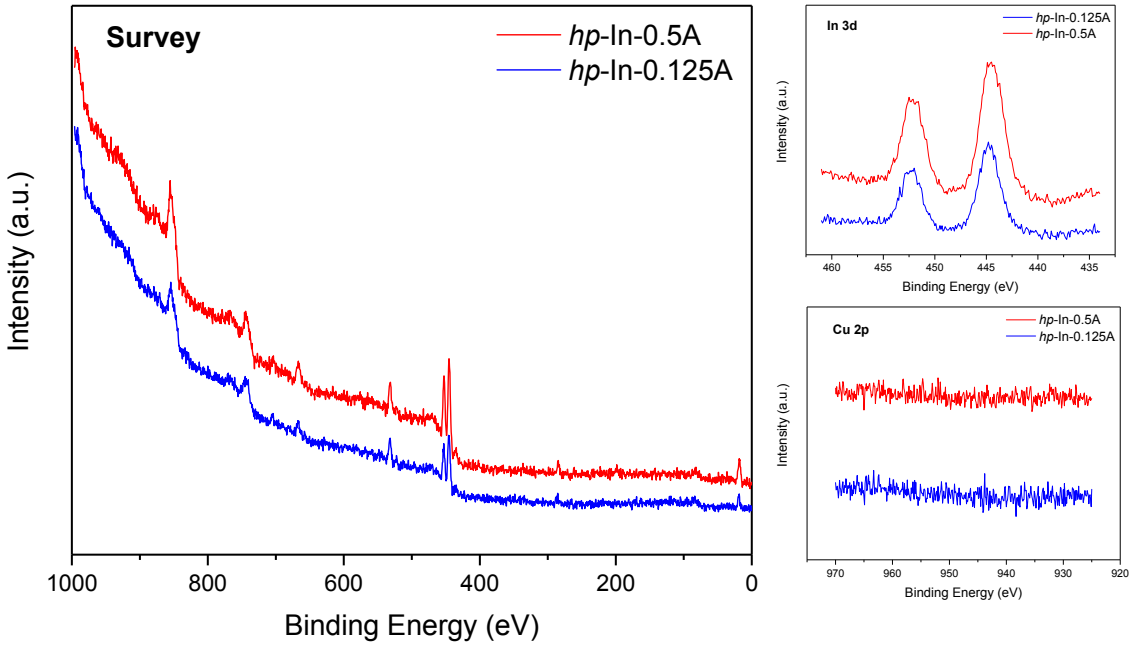

Figure S12 XPS survey, In 3d and Cu 2p spectra of as-prepared *hp*-In-0.125 and *hp*-In-0.5. Although the SEM images show that the porous In was not homogeneous deposited on these two samples at low current densities (Figure S10), XPS spectra indicate that the Cu mesh was fully covered by a layer of In.

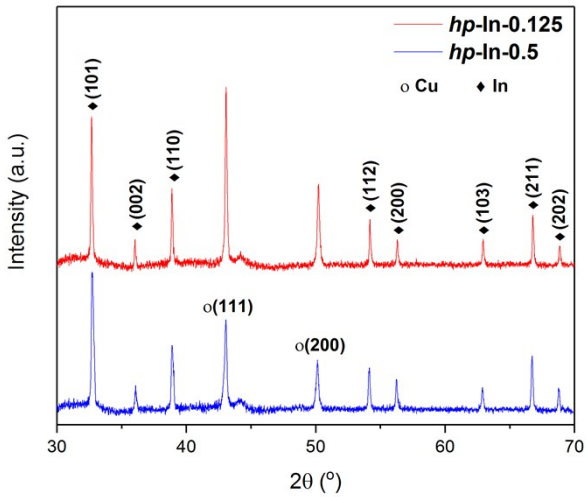

Figure S13 XRD patterns of as-prepared *hp*-In-0.125 and *hp*-In-0.5.

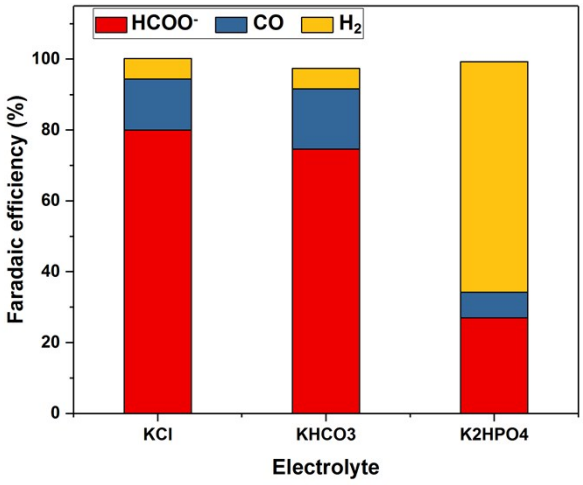

Figure S14 FEs of formate, CO and H_2 for hp-In measured in CO_2 saturated 0.1 M KCl, 0.1 M $KHCO_3$ and 0.1 M K_2HPO_4 at 7 mA/cm^2.

The local pH effect was further confirmed by performing CO_2RR in three different electrolyte with different buffer abilities (i.e., 0.1 M K_2HPO_4 > 0.1M $KHCO_3$ > 0.1M $KClO_4$). Figure S14 shows the FE of H_2 significantly increased when K_2HPO_4, a strong buffer electrolyte, was used instead of $KHCO_3$. In KCl electrolyte, the H_2 FE is similar as that in $KHCO_3$. This may be because the local pH in $KHCO_3$ is already quite high that limits the H_2 FE to only 5.8 %. Thus, the results shown here confirm that the high local pH created near *hp*-In could suppress H_2 evolution and therefore increase the CO_2RR FEs.

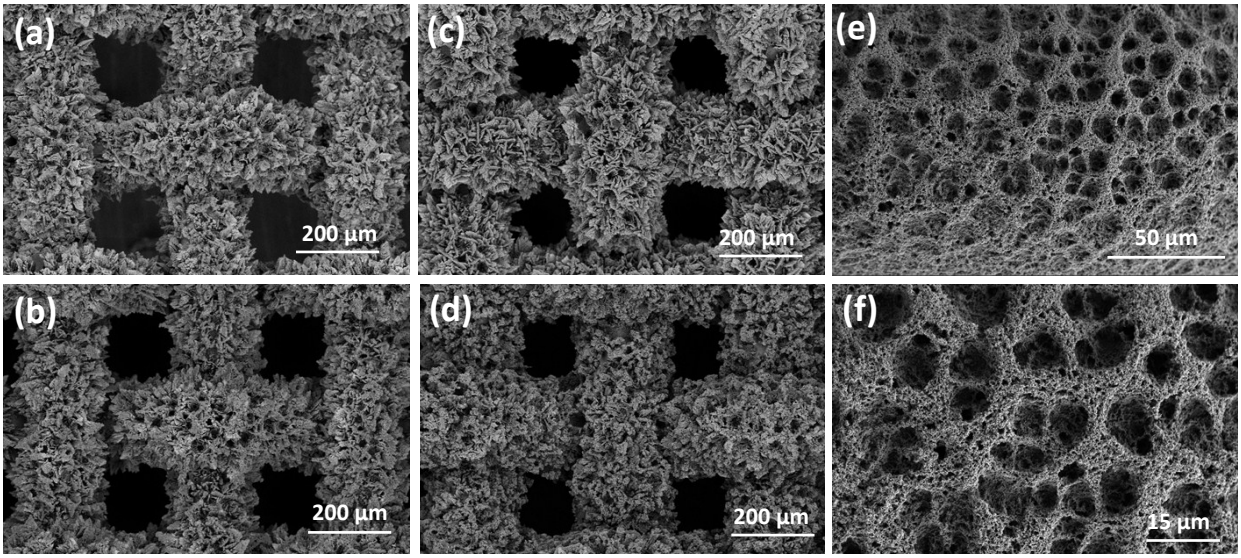

Figure S15 SEM images of Pd-In electrodes treated by different $PdCl_2$ solutions (a) 0.1 mM, (b) 0.5 mM, (c) 1.0 mM and (d) 2.0 mM, and porous Pd electrode with different magnifications (e) and (f).

References:

1 M. Pourbaix, *Atlas of electrochemical equilibria in aqueous solutions*, National Association of Corrosion Engineers, Houston, Tex, 2nd edn., 1974.

2 Y.-H. Chung and C.-W. Lee, *J. Electrochem. Sci. Technol.*, 2012, **3**, 1–13.

3 Z. Bitar, A. Fecant, E. Trela-Baudot, S. Chardon-Noblat and D. Pasquier, *Appl. Catal. B Environ.*, 2016, **189**, 172–180.

4 R. Hegner, L. F. M. Rosa and F. Harnisch, *Appl. Catal. B Environ.*, 2018, **238**, 546–556.

5 Z. Xia, M. Freeman, D. Zhang, B. Yang, L. Lei, Z. Li and Y. Hou, *ChemElectroChem*, 2018, **5**, 253–259.

6 Z. M. Detweiler, J. L. White, S. L. Bernasek and A. B. Bocarsly, *Langmuir*, 2014, **30**, 7593–7600.

7 A. Rabiee and D. Nematollahi, *Mater. Chem. Phys.*, 2017, **193**, 109–116.

8 J. L. White and A. B. Bocarsly, *J. Electrochem. Soc.*, 2016, **163**, H410–H416.

9 C. Ding, A. Li, S. M. Lu, H. Zhang and C. Li, *ACS Catal.*, 2016, **6**, 6438–6443.

10 J. K. Nørskov, T. Bligaard, A. Logadottir, J. R. Kitchin, J. G. Chen, S. Pandelov and U. Stimming, *J. Electrochem. Soc.*, 2005, **152**, J23.

11 P. Wang, X. Zhang, J. Zhang, S. Wan, S. Guo, G. Lu, J. Yao and X. Huang, *Nat. Commun.*, 2017, **8**, 14580.